# Omnidirectional Chargability with Directional Antennas

Haipeng Dai\* Xiaoyu Wang\* Alex X. Liu\*† Fengmin Zhang\* Yang Zhao\* Guihai Chen\*‡

\*State Key Laboratory for Novel Software Technology, Nanjing University, Nanjing, Jiangsu 210024, CHINA

†Department of Computer Science and Engineering, Michigan State University, East Lansing, MI, USA

‡Shanghai key Laboratory of Scalable Computing and Systems, Shanghai Jiao Tong University, Shanghai 200240, CHINA
{haipengdai,gchen}@nju.edu.cn,wangxiaoy51448@yahoo.com, alexliu@cse.msu.edu,{zfm199006,youngzh1993}@163.com

Abstract—Wireless Power Transfer (WPT) has received more and more attentions because of its convenience and reliability. In this paper, we first propose the notion of omnidirectional charging by which an area is omnidirectionally charged if a device with directional antennas at any position in the area with any orientation can be charged by directional chargers with power being no smaller than a given threshold. We present our empirical charging model based on field experimental results using off-theshelf WPT products. Next, we consider the problem of detecting whether the target area achieves omnidirectional charging given a deterministic deployment of chargers. We develop piecewise constant approximation and area discretization techniques to partition the target area into subareas and approximate powers from chargers as constants. Then we propose the Minimum Coverage Set extraction technique which reduces the continuous search space to a discrete one and thereby allows a fast detection algorithm. Moreover, we consider the problem of determining the probability that the target area achieves omnidirectional charging given a random deployment of chargers. We first replace the target area by grid points on triangular lattices to reduce the search space from infinite to finite, then approximate chargers' power with reasonable relaxation, and derive an upper bound of the omnidirectional charging probability. Finally, we conduct both simulation and field experiments, and the results show that our algorithm outperforms comparison algorithms by at least 120%, and the consistency degree of our theoretical results and field experimental results is larger than 93.6%.

#### I. INTRODUCTION

#### A. Motivation and Problem Statement

Nowadays, Wireless Power Transfer (WPT) has received more and more attentions from both academic and industrial circles due to its convenience of no wiring and contactless and reliability of power supply. Many WPT systems for scientific research purposes such as the industrial wireless identification and sensing platform (WISP) [1] are designed and implemented, and the member companies of Wireless Power Consortium that aims to promote the standardization of WPT has grown to 228 in 2016 and involves companies like Microsoft, Huawei and Samsung. One critical and practical issue for WPT is that when the angle of the orientations of a wireless directional charger with a charging sector area and a rechargeable device with a directional antenna is larger than a given threshold, the device can not receive any power. For example, in Fig. 1, the device  $s_i$  can receive a non-zero power form the wireless charger  $o_i$  while  $s_k$  can not. Moreover, considering the potential mobility of devices, a device may

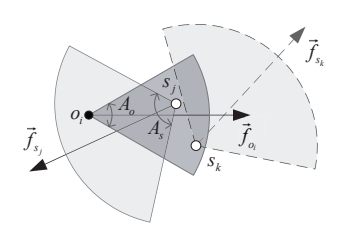




Fig. 1: Directional charging model

Fig. 2: Omnidirectional charging for an area  $\Omega$ 

receive a large enough power at a specific position with a specific orientation, but it may not hold when the device moves to another position or rotates a bit. To provide reliable power supply, we desire that a device can receive a sufficiently large power at any position and with any orientation inside a given area, such as the area  $\Omega$  shown in Fig. 2. Example applications include millimeter wave cellular networks [2], [3], wireless rechargeable sensor networks [4] and wireless charging systems adopting the simultaneous wireless information and power transfer technology [5], [6], all of which consist of transmitters and receivers equipped with directional antennas. Further, wireless chargers can be regarded as randomly deployed in some scenarios, such as power beacons or base stations in cellular networks [7], [8], or base stations in millimeter wave networks [6] that suffer from blockage effects resulting from buildings in urban areas. Therefore, we consider two different cases in this paper, namely, chargers are deterministically deployed or randomly deployed.

In this paper, we first propose the notion of *omnidirectional* charging and say an area is omnidirectionally charged if a device at any point in the area with any orientation can be charged with power being no smaller than a given threshold. We present the empirical charging model based on our experimental results using off-the-shelf WPT products. Next, we consider two fundamental problems of omnidirectional charging. First, given a deterministic deployment of directional chargers, we want to detect whether every point in the target area is omnidirectionally charged, or we say the target area achieves omnidirectional charging. Second, given a random deployment of directional chargers where chargers are uniformly distributed, we wish to calculate the probability that the target area achieves omnidirectional charging.

#### B. Limitations of Prior Art

Though there have emerged some literatures studied the wireless charger networks, none of them considered omnidirectional charging. All these literatures assume an omnidirectional power receiving model for devices, that is, no matter which direction the device faces, it receives constant power, and focus on optimizing the charging efficiency of devices [9]–[14]. Note that some of these literatures, *e.g.*, [14], considered the directional charging model rather than omnidirectional charging model for wireless chargers. This merely makes the disk charging area of chargers become sectors, and the considered problem itself is still essentially a coverage problem. Therefore, the approaches proposed in these works can not be adapted to address our problem.

#### C. Technical Challenges

The first technical challenge is that the charging powers from wireless chargers are nonlinear with distance, and the received power of each device is the aggregated powers from all chargers, rendering both of the considered problems nonlinear. Even worse, the positions of chargers for random deployments studied in the second problem are assumed to be random variables rather than deterministic ones, which aggravates the difficulty of theoretical analysis. Second, the search space for either positions or orientations of devices is continuous, which implies an infinite number of candidate instances need to be checked.

#### D. Proposed Approaches

For the first problem, we develop piecewise constant approximation and area discretization techniques to partition the target area into subareas, and approximate the nonlinear powers for every charger in a given subarea as a constant value with bounded approximation errors. Therefore, we convert the original nonlinear problem with continuous search space into a number of linear subproblems with smaller continuous search space which are much easier to be handled, and thus address the first challenge. Then, we propose a so-called Minimum Coverage Set extraction technique to reduce the continuous search space for each subproblem to a discrete one with a limited number of points in the target area to be checked, which provably has no performance loss and leads to a fast detection algorithm for omnidirectional charging. Thereby we overcome the second challenge.

For the second problem, we first transform the receiving power analysis for any point in the area, which is required for omnidirectional charging detection, to that for a limited number of grid points at triangular lattices. This addresses the second challenge. Next, we address the first challenge by approximating charger's power with moderate relaxation, which enables a closed form expression for the aggregate power for a random point in the target area. Based on this result, we derive the upper bound of the probability that all these grid points are omnidirectionally charged, which can be regarded as the omnidirectional charging probability of the whole area.

#### E. Evaluation Results

We conducted extensive simulations and field experiments to verify our theoretical findings. The simulation results show that our algorithm outperforms comparison algorithms, including an adapted algorithm based on the full-view detection algorithm in wireless sensor networks, by at least 120%, and our upper bound for omnidirectional charging probability for random deployment holds. The field experimental results show that the consistency degree of our theoretical results and field experimental results is larger than 93.6%.

#### II. RELATED WORK

Wireless charger networks. Most literatures studying wireless charger networks focus on maximizing the overall charging utility of the network, but none of them considers the omnidirectional charging problem. He et al. [9] and Zhang et al. [10] studied the wireless charger deployment problem, and aimed to maximize the sum of all utilized charging power of devices. Moreover, Dai et al. first took into consideration the high electromagnetic radiation (EMR) caused by wireless charging and presented the safe charging problem. Their goal is to optimize the charging efficiency for chargers with adjustable power [11] or not [12] while guaranteeing that no point on the plane exceeds the EMR safety threshold. Nikoletseas [13] considered more realistic factors such as energy storage capacity of rechargeable nodes for the safe charging problem. All the above-mentioned related works assumed omnidirectional charging models for both wireless chargers and rechargeable devices, which can not be adapted to address our problem.

Full-view coverage in wireless sensor networks (WSNs). Full-view coverage in WSNs is most relevant to our problem. It refers to the case that for any direction with respect to a considered object, there always exists a directional sensor that covers the object, and the angle between the sensor's viewing direction and the object's facing direction is no larger than a given threshold. Wang et al. [15] first presented the notion of full-view coverage, and studied full-view coverage detection in any given camera sensor networks. Wu et al. [16] studied the full-view coverage problem with randomly deployed heterogeneous camera sensors, and Hu et al. [17] extended the full-view coverage analysis to mobile scenarios. Wang et al. [18] proposed the first full-view coverage scheme in barrier coverage context, which is improved by Yu et al. [19] in terms of the required camera sensors. Basically, fullview coverage detection is essentially a linear and geometric problem, and their solutions can not be employed to address the nonlinear problems in this paper.

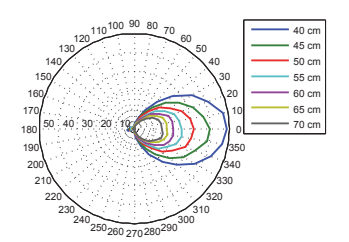
#### III. NOTATIONS AND MODEL

#### A. Network Model

Suppose we have N directional wireless chargers denoted as  $O=\{o_1,o_2,...,o_N\}$  in a bounded area  $\Omega$  with fixed known positions. Moreover, there are also a set of homogeneous rechargeable devices  $S=\{s_1,s_2,...,s_M\}$  scattered in the same area  $\Omega$ , each of which is able to harvest energy via wireless from wireless chargers in O to sustain their normal

TABLE I: Notations

Symbol	Meaning
$o_i$	Wireless charger $o_i$
$s_{j}$	Rechargeable device $s_i$
$A_o$	Charging angle of chargers
$A_s$	Receiving angle of devices
$P_r(d)$	Charging power from distance d
$P_{th}$	Threshold of omnidirectional charging
$\alpha, \beta$	Constants in the charging model
D	Farthest distance a charger can reach



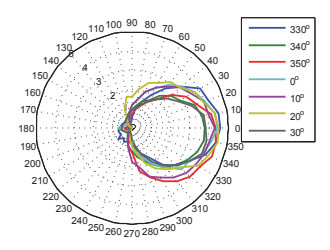


Fig. 3: Charging power vs. distance

Fig. 4: Charging power vs. orientation angle

working. Without confusion, we use  $o_i$  (i=1,2,...,N) and  $s_j$  (j=1,2,...,M) to denote the position of the charger  $o_i$  and the device  $s_j$ , respectively.

All notations used in this paper are listed in Table I.

#### B. Charging Model

We build our charging model by empirical studies in terms of distance between chargers and devices, and orientations of chargers and devices. The testbed is composed of a commodity off-the-shelf wireless charger TX91501 produced by Powercast [20], and a rechargeable sensor node equipped with a  $915\,MHz$  directional PCB patch antenna.

First of all, we vary the distance of the sensor node from 40 cm to 70 cm, the charger's orientation angle with respect to the line connecting the charger and the node from  $0^{\circ}$  to 360°, and set the device facing to the charger. Fig. 3 shows the results, and we can see the node can receive notable power from the charger only when it is within the span of a 60° sector faced by the charger, while in contrast the power received elsewhere, especially that at the back of the charger, is negligibly small. Next, we fix the distance between the charger and the sensor node as 1 m, and vary the charger's orientation angle with respect to the line connecting the charger and the node from  $-30^{\circ}$  (330°) to 30°, and the node's orientation angle with respect to the line connecting the node and the charger from  $0^{\circ}$  to  $350^{\circ}$ . The result is demonstrated in Fig. 4. It can be seen that the node can receive notable charging power only when the orientation angle with respect to the line connecting the node and the charger is within the range from  $-60^{\circ}$  to  $60^{\circ}$ .

Based on the above experimental results, we propose our directional charging model as shown in Fig. 1. We assume that a charger, say  $o_i$ , with orientation vector  $\overrightarrow{f_{o_i}}$  charges devices, e.g.,  $s_j$ , in a charging area in the shape of a sector with charging angle  $A_o$  and radius D. The charging power outside the sector area is zero. Similarly, the rechargeable device also has a (power) receiving area in the shape of a sector with a

(power) receiving angle  $A_s$  and the same radius D.

To summarize, the conditions that a device  $s_j$  can receive a non-zero charging power from a charger  $o_i$  is that  $s_j$  and  $o_i$  should be located in the charging area of  $o_i$ , and the receiving area of  $s_j$ , respectively, which can be mathematically expressed as: (1)  $||o_is_j|| \leq D$ ; (2)  $<\overrightarrow{f_{o_i}}, \overrightarrow{o_is_j}> \leq A_o/2$ ; and (3)  $<\overrightarrow{f_{s_j}}, \overrightarrow{s_jo_i}> \leq A_s/2$ . Here  $||o_is_j||$  denotes the distance between  $o_i$  and  $s_j$ , and the notation  $<\overrightarrow{a}, \overrightarrow{b}> \in [0^\circ, 180^\circ]$  denotes the angle between two vectors  $\overrightarrow{a}$  and  $\overrightarrow{b}$ . Taking Fig. 1 as an example,  $s_j$  can receive power from  $o_i$  while  $s_k$  can not by verifying these three conditions. If these three conditions hold, by adopting the widely accepted empirical charging model [9], [12] and also following our experimental results, the charging power from the charger  $o_i$  to the device  $s_j$  is given by:

$$P_r(||o_i s_j||) = \begin{cases} \frac{\alpha}{(||o_i s_j|| + \beta)^2}, & 0 \le ||o_i s_j|| \le D\\ 0, & ||o_i s_j|| > D \end{cases}$$
(1)

where  $\alpha$  and  $\beta$  are two constants depending on the magnetic environment and the charger's hardware parameters [9], [12], [21], and  $||o_is_j||$  represents the distance between  $o_i$  and  $s_j$ . In addition, we assume the charging power is additive [9], [12], [21]. More specifically, when a device  $s_j$  is charged by multiple chargers, the received power of  $s_j$  is the sum of the received power from all chargers.

#### C. Omnidirectional Charging Definition

In this subsection, we first give some necessary definitions and then introduce the concept of omnidirectional charging.

**Definition** 3.1: (strategy) A strategy for deployment is a two-tuple  $(p, \theta)$   $(p \in \Omega \text{ and } \theta \text{ } (0^{\circ} \leq \theta < 360^{\circ}))$  that denotes the position p and the associated orientation  $\theta$  for deployment.

**Definition** 3.2: Given a device  $s_j$  and a charger  $o_i$ , if  $s_j$  adopting strategy  $(p, \theta)$  can be charged by  $o_i$ , we say  $o_i$  covers  $s_j$ . Further, the covering charger set regarding  $s_j$  adopting strategy  $(p, \theta)$ , or strategy  $(p, \theta)$  for short, is the set of all chargers covering  $s_j$  in the considered area.

**Definition** 3.3: (omnidirectional charging) Given a device and its associated position  $s_j$ , we say  $s_j$  is omnidirectionally charged if the device with any orientation can be charged with a charging power being no smaller than a given threshold  $P_{th}$ . Moreover, an area  $\Omega$  achieves omnidirectional charging if devices with any strategy  $(p,\theta)$   $(p\in\Omega)$  can be omnidirectionally charged.

## IV. OMNIDIRECTIONAL CHARGING DETECTION FOR DETERMINISTIC DEPLOYMENT

In this section, we present our approach to detect whether a given deterministic network of chargers and devices achieves omnidirectional charging. In particular, we first develop an area discretization approach to convert the original nonlinear problem with continuous search space into a number of linear subproblems with smaller continuous search space which are much easier to be handled. Then, we propose a so-called Minimum Coverage Set extraction technique to reduce the continuous search space for each subproblem to a discrete

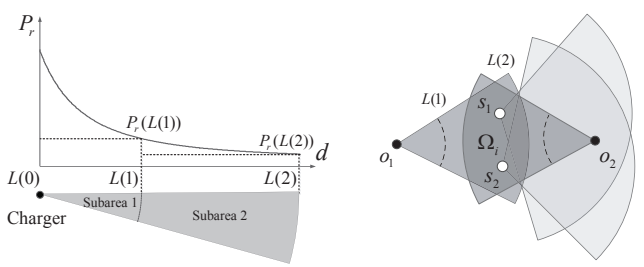


Fig. 5: Power approximation

Fig. 6: Area discretization

one with a limited number of strategies, which allows fast detection of omnidirectional charging.

#### A. Area Discretization

In this subsection, we use an area discretization technique to partition the area into multiple subareas. Our objective is to decompose the original nonlinear problem into many linear subproblems which are easier to be addressed.

1) Piecewise Constant Approximation of  $P_r(d)$ : Basically, we use multiple piecewise constant segments  $P_r(d)$  to approximate the charging power  $P_r(d)$ , which serves as a basis for area discretization. Our goal is to bound the approximation error and the computational overhead.

Fig. 5 illustrates the key idea of the approximation of  $P_r(d)$ . Let  $L(0), L(1), \ldots, L(K)$  be the end points of K constant segments in an increasing sequence. Here, K is the number of segments that controls the approximation error. Obviously, with a larger K, the approximation error will be reduced, but more computational overhead will be introduced. In Fig. 5, K is set to 2, and the horizontal dotted curves stand for the approximated value of charging power.

**Definition** 4.1: Setting L(0) = 0 and L(K) = D, the piecewise constant function  $P_r(d)$  can be defined as

$$\widetilde{P}_r(d) = \begin{cases} P_r(L(1)), & d = L(0) \\ P_r(L(k)), & L(k-1) < d \le L(k) \ (k = 1, \dots K) \\ 0, & d > L(K) \end{cases}$$

Furthermore, the following theorem offers the sufficient condition to ensure that the approximation error is less than  $\epsilon$ . Note that we omit the proofs of some theorems and lemmas in this paper to save space.

**Theorem** 4.1: Setting L(0) = 0, L(K) = D, and L(k) = $\beta((1+\epsilon)^{k/2}-1), (k=1,...,K-1),$  we have the approximation error as

$$1 \le \frac{P_r(d)}{\widetilde{P}_r(d)} \le 1 + \epsilon, \ (d \le D). \tag{2}$$

**Theorem** 4.2: The number of constant segments  $K \lceil \frac{\ln(P_r(0)/P_r(D))}{\ln(1+\epsilon)} \rceil$ . In other words, we have  $K = O(\epsilon^{-1})$ .

2) Discretizing the 2D Area: In this subsection, we demonstrate how to discretize the 2D area based on the piecewise constant approximation of  $P_r(d)$ , and confine the solution

The basic idea of area discretization is shown in Fig. 6. We draw concentric and radius coincided sectors with radius L(1), L(2), ..., L(K) centered at each charger respectively according to each charger's coverage area discretization. In Fig. 6, both of devices  $s_1$  and  $s_2$  fall between two sectors with radius L(1) and L(2) centered at the charger  $o_2$ , and are covered by  $o_2$ . Therefore, the approximated charging power for  $s_1$  and  $s_2$  from charger  $o_2$  is identical and is equal to  $P_r(L(2))$ . By this approach, the whole 2D plane is partitioned into a number of subareas. In Fig. 6, the aggregate charging area of two chargers  $o_1$  and  $o_2$  is partitioned into 9 subareas.

With all these, we can bound the approximation error of charging power for devices, as well as the number of partitioned subareas.

**Theorem** 4.3: Let  $P_r(s_j)$  be the approximated charging power of device  $s_j$ , namely,  $\tilde{P}_r(s_j) = \sum_{i=1}^N x_{ji} \tilde{P}_r(||o_i s_j||)$ , where  $x_{ji} = 1$  if  $s_j$  can be charged by  $o_i$  and  $x_{ji} = 0$  otherwise, we have the approximation error as  $1 \leq \frac{P_r(s_j)}{\tilde{P}_r(s_j)} \leq 1 + \epsilon$ . Proof: Following from Eq. (2), the approximation error

satisfies

$$\frac{P_r(s_j)}{\widetilde{P}_r(s_j)} = \frac{\sum_{i=1}^{N} x_{ji} P_r(||o_i s_j||)}{\sum_{i=1}^{N} x_{ji} \widetilde{P}_r(||o_i s_j||)} \le 1 + \epsilon, \tag{3}$$

as well as  $\frac{P_r(s_j)}{\widetilde{P}_r(s_j)} \geq 1$ . Then the result follows. **Lemma** 4.1: The number of subareas Z partitioned by n

uniform sectors is subject to  $Z \leq 5n^2 - 5n + 2$ .

**Theorem** 4.4: The number of partitioned subareas is subject to  $Z = O(N^2 \epsilon^{-2})$ .

*Proof:* Obviously, given N chargers, there will be at most NK sectors which may intersect with each other. Following Theorem 4.2 and Lemma 4.1, we have  $K = O(\epsilon^{-1})$ , and the number of subareas  $Z \leq 5(NK)^2 - 5NK + 2$ , which means  $Z = O(N^2 \epsilon^{-2}).$ 

Next, we consider the strategies in each subarea.

#### B. Minimum Coverage Set (MCS) Extraction

After the area discretization, the nonlinear powers from chargers to their surrounding devices are approximated to be constant within the same subarea, which greatly eases the problem as it becomes a linear one. Nevertheless, the search space of the problem is still infinite as a subarea has an infinite number of strategies with arbitrary positions and orientations. To address this challenge, we propose an approach of extracting only a finite number of strategies associated with some representative covering charger sets, i.e., Minimum Coverage Sets (MCSs), which guarantee to contain the one yielding the minimum charging power in the considered subarea. Finally, we make a global decision on omnidirectional charging based on the obtained results for all subareas.

In this section, we first present some necessary definitions to assist further analysis, then introduce the MCS extraction method for point cases, and extend it to area cases.

1) Preliminaries: To begin with, we give the following definitions.

Definition 4.2: (Minimum Coverage Set) Given a subarea and a set of chargers  $O_i$  each in which is able to cover a same device placed in the subarea, if there doesn't exist a set O<sub>i</sub>  $(O_j \neq O_i)$  covering a certain device in the same subarea such that  $O_i \subset O_i$  then  $O_i$  is a Minimum Coverage Set (MCS).

Fig. 7: A toy example of MCS extraction for area cases

Fig. 8: Boundary condition

**Definition** 4.3: Given two strategies  $(p_1, \theta_1)$ ,  $(p_2, \theta_2)$  in the same subarea and their corresponding covering charger sets  $O_1$  and  $O_2$ , if  $O_1$  equals  $O_2$ , then  $(p_1, \theta_1)$  is equivalent to  $(p_2, \theta_2)$ . Further, if  $O_1 \subset O_2$ , then  $(p_1, \theta_1)$  is inferior to  $(p_2, \theta_2)$ .

**Definition** 4.4: The candidate covering charger set  $\widehat{O}_i$  for subarea  $\Omega_i$  are those chargers that can cover devices in  $\Omega_i$  with certain orientations.

Clearly, instead of enumerating all possible strategies and their associated covering charger sets in a given subarea, we only have to consider all MCSs because they must contain one leading to the minimum charging power. In what follows, we first consider MCS extraction for a special case in which a subarea reduces to a point, in order to facilitate the following analysis, then we study the general case.

- 2) MCS Extraction for Point Cases: The basic idea of MCS extraction for point cases is to rotate a virtual device located at the considered point such that its orientation angle varies from  $0^{\circ}$  to  $360^{\circ}$ , and record the minimum covering charger sets during this process as MCSs. Due to space limit, we omit the details of the algorithm here to save space.
- 3) MCS Extraction for Area Cases: Next, we consider how to extract MCSs given a general subarea  $\Omega_i$ .

We present the details of the algorithm in Algorithm 1. Fig. 7 shows an example of how the algorithm operates. Given 6 chargers and a subarea as Fig. 7(a) demonstrates, we first draw lines passing through each pair of chargers, such as  $o_1$ and  $o_2$  shown in Fig. 7(b1), and cross the boundaries of the subarea at points p' and p'', centered at which we plot two sectors with fan angle  $A_s + \delta$ , where  $\delta$  is a predefined small positive value that can be arbitrarily close to 0°. Then we shrink the fan angles of these two sectors from  $A_s + \delta$  to  $A_s$ without changing the orientation to exclude the two points  $o_1$ and  $o_2$  (shown in Fig. 7(b2)) and obtain two MCSs  $\{o_3, o_5, o_6\}$ and  $\{o_3, o_4, o_5, o_6\}$ . Next, we also draw arcs passing each pair of chargers such as  $o_3$  and  $o_4$  with a circumferential angle  $A_s + \delta$  and crossing the boundaries of the subarea at points p' and p'' as shown in Fig. 7(c1), and then establish two sectors with fan angle  $A_s + \delta$ . Similarly, we shrink their fan angles to  $A_s$  without changing the orientation to exclude  $o_3$  and  $o_4$ , and thereby find two identical MCSs  $\{o_5, o_6\}$  as illustrated in Fig. 7(c2). After that, we randomly choose a point  $p_{ref}$ on the boundaries, as shown in Fig. 7(d), and perform MCS extraction for point cases to further find MCSs. At the final step,  $\{o_3, o_4, o_5, o_6\}$  and  $\{o_3, o_5, o_6\}$  can be removed as they are supersets of MCS  $\{o_5, o_6\}$ .

Algorithm 1 has two significant features. One is that the

#### Algorithm 1: MCS Extraction for Area Cases

**Input**: The subarea  $\Omega_i$ , the candidate covering charger set  $\widehat{O}_i$  **Output**: All MCSs

- 1 for all pairs of chargers, say  $o_1$  and  $o_2$ , in  $\widehat{O}_i$  do
- Draw a straight line passing through  $o_1$  and  $o_2$  and extend the line to intersect with the subarea's boundaries. Place devices at these intersection points and adjust their orientations such that  $o_1$  and  $o_2$  lies rightly on the anticlockwise boundary of a coverage sector with fan angle  $A_s + \delta$  ( $\delta$  is a predefined small positive value that can be arbitrarily close to  $0^{\circ}$ ). Then shrink the fan angle of these sectors to  $A_s$  and compute the MCSs under the current setting and insert them into the candidate MCS set. If there exists an empty set among the MCSs, return an empty MCS.
- Draw two arcs passing through  $o_1$  and  $o_2$  with a circumferential angle of  $A_s + \delta$  with respect to them, and find the intersection points of the trajectory and the subarea's boundaries. Place devices at these intersection points and adjust their orientations such that  $o_1$  and  $o_2$  lie rightly on sector's two line boundaries, respectively. Then shrink the fan angle to  $A_s$ , and compute the MCSs under this setting and insert them into the candidate MCS set. If there is an empty set in the MCSs, return an empty MCS.
- 4 Randomly select a point  $p_{ref}$  at the boundary of the subarea, perform MCS extraction for point cases and add the results to the candidate MCS set.
- 5 Identify and remove all the MCSs which contain other MCSs in the candidate MCS set.

algorithm only considers the strategies with points on the boundaries, rather than those inside the subarea. The other is that only a limited number of points on the boundaries are considered. We will show that why such approach is sufficient to extract all MCSs for the subarea. Before that, we give an observation and some necessary definitions first.

**Observation** 4.1: For any charger  $o_i$  in a candidate covering charger set  $\widehat{O}_i$  associated with a subarea  $\Omega_i$ ,  $\Omega_i$  must lie between its two concentric sectors with radius L(k-1) and K(k)  $(1 \le k \le K)$ , and any device  $s_j$  in  $\Omega_i$  with  $(1 \le k \le K)$  must be charged by  $o_i$  with power  $(1 \le K)$ .

Next, we define three transformations of strategies.

**Definition** 4.5: (projection) Given a strategy  $(p, \theta)$ , move the device along the direction of its orientation until reaching some point p' on the boundary of the subarea, while keeping its orientation unchanged.

**Definition** 4.6: (rotation) Given a strategy  $(p, \theta)$ , rotate the device from  $\theta$  to  $\theta'$  and keep the position unchanged.

**Definition** 4.7: (translation) Given a strategy  $(p, \theta)$ , move the device from the position p to another position p' and keep

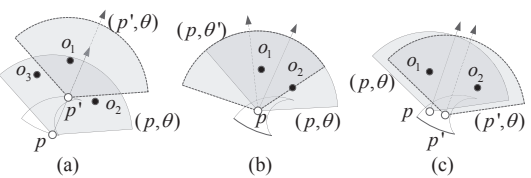


Fig. 9: Three kinds of transformation: (a) projection, (b) rotation, (c) translation

the orientation unchanged.

Fig. 9 demonstrates these three transformations. For projection transformation, we have the following lemma.

**Lemma** 4.2: If  $(p', \theta)$  is the projection of  $(p, \theta)$ , then  $(p', \theta)$  is either equivalent or inferior to  $(p, \theta)$ .

*Proof:* Suppose there is a charger  $o_1$  covering strategy  $(p,\theta)$  where p is a position inside the subarea  $\Omega_i$ , as is shown in Fig. 8. We then connect p and  $o_1$  as well as p' and  $o_1$ . Let  $\psi, \psi'$  denote the angles between  $po_1, p'o_1$  and the orientation of the strategy, respectively. It is obvious that  $\psi'$  is larger than  $\psi$  since  $\psi' = \psi + \angle po_1p'$ . So,  $\psi \leq A_s/2$  does not necessarily lead to  $\psi' \leq A_s/2$ , which means  $o_1$  may not cover  $(p',\theta)$  even it covers  $(p,\theta)$ . In contrast, if  $o_1$  covers  $(p',\theta)$ , it must also cover  $(p,\theta)$  because of  $\psi < \psi' \leq A_s/2$  and Observation 4.1. Therefore,  $(p',\theta)$  must be equivalent or inferior to  $(p,\theta)$ .

Fig. 9(a) shows an example that after the projection transformation, the device at the new position p' can only cover  $o_3$  instead of  $o_1$ ,  $o_2$  and  $o_3$ . According to Lemma 4.2, we can easily get the following crucial corollary.

**Corollary** 4.1: It suffices to consider the case in which devices located on the boundaries of a subarea in terms of MCS extraction.

Furthermore, we introduce the following critical theorem for MCS extraction.

**Theorem** 4.5: Given a subarea  $\Omega_i$ , the output MCSs of Algorithm 1 contains all possible MCSs for  $\Omega_i$ .

*Proof:* According to Corollary 4.1, we only need to consider strategies with their positions on the boundaries of the subarea.

Given an arbitrary strategy  $(p,\theta)$ , we perform the following two-step adjustments. At the first step, fix the position p, rotate the device anticlockwise to be  $(p,\theta')$  such that there is at least one charger outside the receiving area of the device, say  $o_2$ , touching the left boundary of the device's receiving area, as shown in Fig. 10(a). A crucial observation of such adjustment is that  $(p,\theta')$  is either equivalent or inferior to  $(p,\theta)$  if all chargers lying on the anticlockwise boundary of the device's receiving area such as  $o_2$  can be excluded.

At the second step, move the device along the subarea's boundaries and change its orientation accordingly, *i.e.*, perform translation and rotation continuously on  $(p, \theta')$ . During such process, we require that the anticlockwise boundary of the device's coverage area must cross  $o_2$ . Clearly, there are only three possible situations encountered when such adjustment proceeds, as shown in Fig. 10.

Case I: At some position p' on the boundary of the subarea, there is some charger (e.g.,  $o_3$  in Fig. 10(a)) that touches the anticlockwise boundary of the coverage area of  $(p', \theta'')$ .

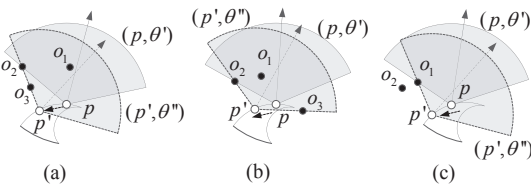


Fig. 10: Three kinds of transformation results

Case II: At some position p' on the boundary of the subarea, there is some charger (e.g.,  $o_3$  in Fig. 10(b)) that touches the clockwise boundary of the coverage area of  $(p', \theta'')$ .

Case III: Neither the situation in (a) nor that in (b) occurs for any position p' on the boundary of the subarea (as shown in Fig. 10(c)).

Indeed, in Case III,  $(p',\theta'')$  is equivalent to  $(p,\theta')$  for any position p' on the subarea's boundaries. Besides, we note that, during the adjustment, it is impossible that a charger is going to fall in the sector area from the arc boundary of the area. This is because by following Observation 4.1, as long as a charger  $o_i \in \widehat{O}_i$  and a device  $s_j$  in the subarea  $\Omega_i$  satisfies  $\langle \overrightarrow{f_{s_j}}, \overrightarrow{s_jo_i} \rangle \leq A_s/2$ ,  $o_i$  must cover  $s_j$ .

A crucial observation of the above adjustments is that, the final obtained strategy  $(p', \theta'')$  after the second step transformation is either equivalent to  $(p, \theta')$  (Case III) or inferior to  $(p, \theta')$  if those new covering chargers touching the anticlockwise or clockwise boundaries of the device's receiving area such as  $o_3$  can be excluded (Case I and II). Combining it with the observation for the first step adjustment, we conclude that  $(p', \theta'')$  is either equivalent or inferior to  $(p, \theta)$  if all chargers lying on the anticlockwise or clockwise boundaries of the device's receiving area can be excluded.

In fact, Step 2, Step 3, and Step 4 in Algorithm 1 exactly correspond to extracting all  $(p',\theta'')$ s for Case I, II, and III and meanwhile excluding all chargers on their boundaries, respectively. In particular, randomly selecting a position on the subarea's boundaries and performing MCS extraction for point cases at Step 4 in Algorithm 1 suffices to find all MCSs corresponding to Case III. Since the original strategy  $(p,\theta)$  is arbitrarily selected, we claim that the output MCSs of Algorithm 1 contains all possible MCSs for  $\Omega_i$ . This completes the proof.

#### C. Omnidirectional Charging Detection

Based on all MCSs extracted from each subarea, the global omnidirectional charging detection is quite straightforward. We only need to check the aggregated charging power from each MCS in each subarea one by one, and see whether it exceeds the power threshold for omnidirectional charging. Only when all MCSs pass such checking can we conclude that the considered area achieves omnidirectional charging.

## V. OMNIDIRECTIONAL CHARGING PROBABILITY ESTIMATION FOR RANDOM DEPLOYMENT

In this section, we consider the omnidirectional charging problem in the context of random deployment. Especially, we focus on analyzing the upper bound of omnidirectional charging probability. Our approach is to first transform the receiving power analysis for any point in the area, which is required for omnidirectional charging detection, to that for a limited number of grid points at triangular lattices, then derive the upper bound of the probability that all these grid points are omnidirectionally charged based on the theoretical result for a random point.

#### A. Problem Transformation

We approximate the continuous area by discrete grid points that are the vertices of triangle lattices as in [15]. We show in the lemma below that if the grids are sufficiently dense and are all omnidirectionally charged, then the whole area achieves omnidirectional charging. Note that we use a three-tuple  $(D, \phi_s, P_{th})$  to denote the uniform setting of the network in the considered area, where  $\phi_s = A_s/2$  and  $A_o = 2\pi$ .

**Lemma** 5.1: Given that all grid points can be omnidirectionally charged by a set of chargers with setting  $(D', \phi'_s, P'_{th})$  where  $D' = D - \Delta D$ ,  $\phi'_s = \phi_s - \Delta \phi_s$  and  $P'_{th} = P_{th} + \Delta P$  for some given  $(\Delta D, \Delta \phi_s, \Delta P)$ . If the triangle lattice side length  $l \leq l_0(\Delta D, \Delta \phi_s) \triangleq \frac{2\Delta D}{\sqrt{3} + \cot \Delta \phi_s}$  and  $\Delta P \geq \frac{P_r(0) - P_r(\Delta D)}{P_r(\Delta D)}$ , then any point in the area is omnidirectionally charged by the same set of chargers with setting  $(D, \phi_s, P_{th})$ .

*Proof:* According to Lemma 4.1 in [15], the setting  $(D',\phi'_s,P'_{th})$ , together with the triangle lattice side length satisfying  $l \leq \frac{2\Delta D}{\sqrt{3+\cot\Delta\phi_s}}$ , ensures the so-called omnidirectional coverage for the whole area, which can be interpreted as that any strategy in the area can be covered by at least one charger in our context. Hence, we only need to check whether charging powers for all strategies exceed the threshold  $P_{th}$ .

First, by Lemma 4.1 and 4.2 in [15], for any point V in the area, there must exist a grid point  $V_p$  such that  $||V_pV|| \leq \Delta D$ ; further, if there are n chargers covering a device at  $V_p$ , they can also cover a device at V. Though there may be additional chargers cover V, we consider the worst case that no such charger exist and V is only covered by these n chargers. Suppose these n chargers provide  $P_r^1(V), P_r^2(V), ..., P_r^n(V)$  power for a device at V, and  $P_r^1(V_p), P_r^2(V_p), ..., P_r^n(V_p)$  power for a device at  $V_p$ , respectively. From Eq. (1), it is easy to check that the maximum ratio of increased power to original power when moving a device for distance  $\Delta D$  within a charger's charging area is  $\frac{P_r(0)-P_r(\Delta D)}{P_r(\Delta D)}$ . Consequently, we have  $P_r(V_p) = \sum_{i=1}^n P_i^i(V_p) \leq \sum_{i=1}^n [(1+\frac{P_r(0)-P_r(\Delta D)}{P_r(\Delta D)})P_r(V)] = (1+\frac{P_r(0)-P_r(\Delta D)}{P_r(\Delta D)})P_r(V)$ . Furthermore, as  $P'_{th} = P_{th} + \Delta P \geq (1+\frac{P_r(0)-P_r(\Delta D)}{P_r(\Delta D)})P_{th}$ , and  $P_r(V_p) \geq P'_{th}$  because  $V_p$  is omnidirectionally charged given power threshold  $P'_{th}$ , we have  $P_r(V) \geq P_{th}$ .

B. Omnidirectional Charging Probability for a Random Point
To pave the way for studying the omnidirectional charging
probability for all grid points, we consider such probability for
a random point in the considered area. We first present some
useful theoretical results.

**Lemma** 5.2: Given a device that falls in a charger's charging area with radius D', then the probability that the device has distance d to the charger is given by  $f_{dis}(d) = \frac{2d}{D^{72}}$ .

*Proof:* Clearly, the cumulative distribution that a device falls in the area with distance to a charger being no more than

d is  $F_{dis}(d)=rac{\pi d^2}{\pi D'^2}=rac{d^2}{D'^2}.$  Hence, the probability for the device with distance d to the charger is  $rac{\partial F_{dis}(d)}{\partial d}=rac{2d}{D'^2}.$ 

**Lemma** 5.3: By approximating charging power  $P_r(d)$  as

$$P'_r(d) = P_r(d'_0) - \frac{d^2 - d'_0^2}{\gamma D'^2},\tag{4}$$

the probability distribution of charging power in the charging area changes to  $f(P'_r(d)) = \gamma$ ,  $(P_r(D') \leq P'_r(d) < P_r(d'_0))$ , where  $d'_0 = P_r^{-1}(P'_{th})$  and

$$\gamma = \frac{1 - d_0'^2 / D'^2}{P_r(d_0') - P_r(D')}.$$
 (5)

Proof: We can prove this by deriving the cumulative probability  $F_{[d'_0\ d]}(P'_r(d))$  of power from distance  $d'_0$  to d in two different ways. On one hand, it can be computed by integrating all the probability from distance  $d'_0$  to d regarding distance, which means  $F_{[d'_0\ d]}(P'_r(d)) = \int_{d'_0}^d f_{dis}(x) dx = \frac{d^2 - d'_0^2}{D'^2}$  by following Lemma 5.2. On the other hand,  $F_{[d'_0\ d]}(P'_r(d))$  can be also calculated by integrating all the probability from  $f(P'_r(d'_0))$  to  $f(P'_r(d))$  regarding charging power, which means  $F_{[d'_0\ d]}(P'_r(d)) = \int_{P'_r(d'_0)}^{P'_r(d)} f(x) dx = \gamma(P'_r(d) - P'_r(d'_0)) = \frac{d^2 - d'_0^2}{D'^2}$ . These two results are consistent, which validates the correctness of the approximation of charging power in Eq. (4) by setting  $P'_r(d'_0) = P_r(d'_0)$ . Let  $P'_r(D') = P_r(D')$ , we thus obtain  $\gamma$  as shown in Eq. (5).

As a result of such approximation, the probabilistic distribution of power becomes uniform in  $[P_r(D'), P_r(d'_0)]$ , and is equal to  $\frac{1}{P_r(d'_0)-P_r(D')}$  conditioned on  $d \in [d'_0, D']$ , which greatly helps future theoretical analysis. Besides, it is easy to verify that  $P'_r(d) \geq P_r(d)$  for  $d'_0 \leq d \leq D'$ , which means that the approximated power exaggerates the real power.

Next, we present a critical corollary based on the classical result in [22]. We omit the proof to save space.

**Corollary** 5.1: The cumulative distribution of the sum of n random variables that conform to independent and identical distribution  $p = \frac{1}{b-a}$  in the range [a,b] is given by

$$F_Y(y) = \begin{cases} 0, & y < na, \\ \frac{1}{(b-a)^n} \sum_{r=0}^k (-1)^r \frac{[y-na-r(b-a)]^n}{(n-r)!r!}, \\ k(b-a) + na < y \le (k+1)(b-a) + na \\ 1, & y > nb \end{cases}$$
(6)

With all these, we can obtain an upper bound of the omnidirectional charging probability for a single point.

**Lemma** 5.4: Given N chargers with  $A_o=2\pi$  uniformly distributed in an area  $\Omega$  with area  $S_{\Omega}$ , the probability that a device at a random point in  $\Omega$  is omnidirectionally charged is upper bounded by:

$$P_f(N, D', \phi'_s, P'_{th}) = \left(\sum_{m=1}^{N} C_N^m P_1^m (1 - P_1)^{N-m} P_2\right)^{\lfloor \frac{\pi}{\phi'_s} \rfloor},$$
(7)

where 
$$P_1 = \frac{\phi_s' D'^2}{S_D}$$
 and

$$P_{2} = \begin{cases} 1 - \frac{1}{m!} \left[ \frac{(1 - d_{0}^{\prime 2}/D^{\prime 2})(P_{th}^{\prime} - mP_{r}(D^{\prime}))}{(P_{th}^{\prime} - P_{r}(D^{\prime}))} \right]^{m}, \\ mP_{r}(D^{\prime}) < P_{th}^{\prime}, \end{cases}$$
(8)

where  $d'_0 = P_r^{-1}(P'_{th})$ .

*Proof:* First of all, we consider the probability, say  $P_1$ , of a randomly deployed charger covering a given device in an area  $\Omega$ . Clearly,  $P_1$  is exactly equal to the ratio of the size of the charging area to that of the entire area, i.e.,  $P_1 = \frac{\phi_s' D'^2}{S_\Omega}$ . Therefore, the probability that a device can be charged by exactly m chargers follows Binomial distribution and is given by  $C_N^m P_1^m (1-P_1)^{N-m}$  where N is the number of all chargers.

Next, we consider the probability, say  $P_2$ , that a randomly deployed device with a certain orientation in the area is charged with power no less than  $P'_{th}$  from m chargers. Obviously, if  $mP_r(D') \ge P'_{th}$ , these m chargers can definitely jointly charge the device with aggregated power no less than  $P'_{th}$  regardless of their distance to the device, which indicates that  $P_2$  is equal to 1, as shown in Eq. (8).

Otherwise, if  $mP_r(D') < P'_{th}$ , there are only two possible cases: (1) at least one charger provides power no less than  $P'_{th}$ ; and (2) no power from a single charger is no less than  $P'_{th}$ , but the aggregated power from all chargers is. For the former case, as the probability of a device being covered by a charger within distance  $d_0'$  ( $d_0' = P_r^{-1}(P_{th}')$ ) and receiving power no less than  $P_{th}'$  is  $\frac{\phi_s' d_0'^2}{\phi_s' D'^2} = \frac{d_0'^2}{D'^2}$ , its occurrence probability  $P_3$  can be computed as  $P_3 = 1 - (1 - \frac{d_0'^2}{D'^2})^m$ . For the latter case, by similar analysis, we know the probability that no power from a single charger is no less than  $P'_{th}$  is  $(1 - \frac{d'^2_0}{D'^2})^m$ . Further, under this condition, by approximating  $P_r(d)$  as Lemma 5.3 does, the power from each charger becomes uniformly distributed, and therefore by Corollary 5.1, the probability that the aggregated power from all chargers is no less than  $P'_{th}$  is  $1 - F_Y(y)$ , where  $a = P_r(D')$ ,  $b = P_r(d'_0) = P'_{th}$ ,  $y = b = P'_{th}$ , and k satisfies  $\frac{a-ma}{b-a} \le k < \frac{b-ma}{b-a}$ . Clearly, as  $mP_r(D') < P'_{th}$ , namely ma < b, we have  $0 < \frac{b-ma}{b-a} \le 1$ , and therefore k = 0 as k should be a non-negative integer. Finally, we have  $P_2 = P_3 + (1 - \frac{d_0'^2}{D'^2})^m [1 - F_Y(y)]$ . By substituting k = 0, we get Eq. (8) for the case  $mP_r(D') < P'_{th}$ .

As a result, by enumerating all possible number of chargers m, we obtain that the probability for a device with a certain orientation being charged with power no less than  $P'_{th}$  is  $\sum_{m=1}^{N} C_N^m P_1^m (1-P_1)^{N-m} P_2$ . Furthermore, omnidirectional charging requires at least  $\lfloor \frac{\pi}{\phi'_s} \rfloor$  orientations, *i.e.*,  $2\phi'_s$ ,  $2 \cdot 2\phi'_s$ , ...,  $\lfloor \frac{2\pi}{2\phi'} \rfloor \cdot 2\phi'_s$ , to be charged with power exceeding the threshold. Therefore, the whole probability can be expressed as in Eq. (7). After all, as we exaggerate the power  $P_r(d)$ when deriving  $P_2$ , the obtained probability is undoubtedly an upper bound.

C. Omnidirectional Charging Probability for all Grid Points **Theorem** 5.1: Given N chargers with  $A_o = 2\pi$  uniformly distributed in an area  $\Omega$  with size  $S_{\Omega}$ , the probability that

 $P_{2} = \begin{cases} 1 - \frac{1}{m!} \left[ \frac{(1 - d_{0}^{\prime 2}/D^{\prime 2})(P_{th}^{\prime} - mP_{r}(D^{\prime}))}{(P_{th}^{\prime} - P_{r}(D^{\prime}))} \right]^{m}, & \text{Lemma 5.4 and we set } D^{\prime} = \frac{\sqrt{N} - 1}{\sqrt{N}} D, \; \phi_{s}^{\prime}, \; \frac{\sqrt{N} - 1}{\sqrt{N}} \phi_{s}, \\ mP_{r}(D^{\prime}) < P_{th}^{\prime}, & P_{th}^{\prime} = \frac{P_{r}(0)}{P_{r}(D/\sqrt{N})} P_{th}, \; \text{and } G = \left\lceil \frac{2S_{\Omega}}{\sqrt{3}} l_{0}^{-2} \left( \frac{D}{\sqrt{N}}, \frac{\phi_{s}}{\sqrt{N}} \right) \right\rceil \; \text{where}}{l_{0} \; \text{is defined in Lemma 5.1.}} \\ 1, & mP_{r}(D^{\prime}) \geq P_{th}^{\prime}, & P_{th}^{\prime} = \frac{P_{r}(0)}{P_{r}(D/\sqrt{N})} P_{th}^{\prime}, \; \text{and } G = \left\lceil \frac{2S_{\Omega}}{\sqrt{3}} l_{0}^{-2} \left( \frac{D}{\sqrt{N}}, \frac{\phi_{s}}{\sqrt{N}} \right) \right\rceil \; \text{where}}{l_{0} \; \text{is defined in Lemma 5.1.}} \end{cases}$  $\Omega$  achieves omnidirectional charging is upper bounded by

Proof: As the considered area contains in total  $\lceil \frac{S_{\Omega}}{(\sqrt{3}/4)l_0^2(\frac{D}{\sqrt{N}},\frac{\phi_s}{\sqrt{N}})} \rceil = \lceil \frac{4S_{\Omega}}{\sqrt{3}}l_0^{-2}(\frac{D}{\sqrt{N}},\frac{\phi_s}{\sqrt{N}}) \rceil$  triangles and each triangle possesses  $\frac{1}{6} \times 3 = \frac{1}{2}$  grid points on average, the total number of grid points G can be calculated as  $G = \frac{1}{2} S_{\Omega} + \frac{1}{2} S_{$  $\lceil \frac{2S_{\Omega}}{\sqrt{3}} l_0^{-2} (\frac{D}{\sqrt{N}}, \frac{\phi_s}{\sqrt{N}}) \rceil$ . By Lemma 5.4, the probability that a device at a random point in  $\Omega$  is omnidirectionally charged is upper bounded by  $P_f(N, D', \phi'_s, P'_{th})$ . Thus the probability that  $\Omega$  achieves omnidirectional charging is upper bounded by  $P_f(N, D', \phi'_s, P'_{th})^G$ .

#### VI. SIMULATION RESULTS

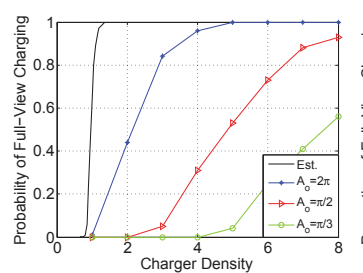
In this section, we conduct simulations to evaluate the performance of our algorithm in terms of the probability and proportion of omnidirectional charging, respectively. The upper bound of omnidirectional charging probability for random deployment is also validated. Moreover, we show the detection time efficiency of our algorithm in comparison with other approaches, and provide insights for the impact of uniformness of position and orientation distributions of chargers.

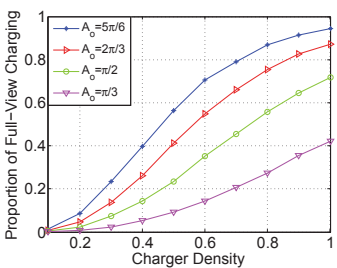
#### A. Evaluation Setup

In our simulation, the target field  $\Omega$  is a  $10 m \times 10 m$  square area, and the chargers are uniformly distributed in this area. We set  $\alpha = 10$ ,  $\beta = 10$ , D = 4,  $P_{th} = 0.06$ , and the error threshold  $\epsilon = 0.3$ . We consider three metrics for evaluation: omnidirectional charging probability, omnidirectional charging proportion, and detection time. Each omnidirectional charging probability result is obtained by averaging results for 100 randomly generated topologies, and each omnidirectional charging proportion result is calculated as the average proportion of omnidirectionally charged grid points on dense triangular lattices with side length  $0.1\,m$  as described in Sec. V for  $100\,$ randomly generated topologies, which can be regarded as a good estimation of the proportion of omnidirectionally charged points on the entire area. For the omnidirectional charging proportion test, the number of chargers varies from 10 to 100, while for the others the number varies from 100 to 800.

#### B. Baseline Setup

As there are no approaches available to detect omnidirectional charging, we devise two algorithms named exhaustive algorithm and omnidirectional coverage algorithm for comparison. The exhaustive algorithm checks every grid point on square lattices to see whether they are omnidirectionally charged. Basically, we consider two settings of side length of square lattices: 0.01 m and 0.02 m. The omnidirectional coverage algorithm is adapted from the traditional omnidirectional coverage algorithm for sensor networks [15] by incorporating some key techniques proposed in our algorithm. Specifically, the algorithm first employs the area discretization technique to partition the area into subareas as we do in Sec. IV-C, and then applies the method in [15] to further divide these





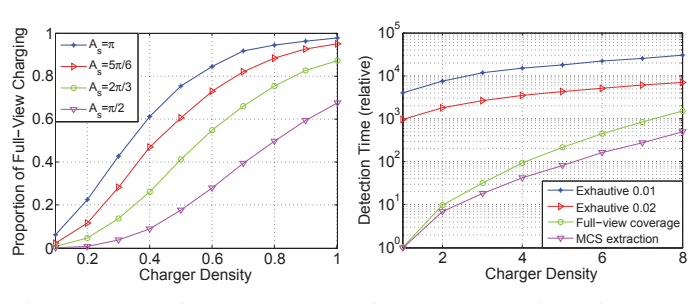


Fig. 11: Probability vs. charger Fig. 12: Proportion vs. charger Fig. 13: Proportion vs. charger Fig. 14: Detection time vs. density density

charger density density

subareas into smaller ones. Next, the algorithm randomly selects a point in each subarea and finds all possible associated covering charger sets, which provably achieves successful omnidirectional charging detection.

### C. Performance Comparison

1) Probability of omnidirectional charging: The simulation results show that our upper bound for omnidirectional charging probability for random deployment holds, and the probability of omnidirectional charging increases when the charger density increases. During the simulation, we fix the device angle  $A_s$  as  $\frac{2\pi}{3}$ . From Fig. 11, we can see our upper bound precisely holds, and the omnidirectional charging probability does not growth uniformly with charging angle  $A_o$ . When  $A_o$ increases from  $\frac{\pi}{3}$  to  $\frac{\pi}{2}$ , the average growth of omnidirectional charging probability is about 62.85%, while  $A_o$  jumps from  $\frac{\pi}{2}$  to  $2\pi$ , the average growth is only 58.94%. This observation indicates a decreasing marginal benefit for increasing charger density in terms of omnidirectional charging probability.

2) Proportion of omnidirectional charging: The simulation results show that the omnidirectional charging proportion increases monotonically with an increasing charger density, charging angle  $A_o$ , or receiving angle  $A_s$ . We respectively fix  $A_s = \frac{2\pi}{3}$  and  $A_o = \frac{2\pi}{3}$  and plot the simulation results in Fig. 12 and 13. It can be seen that the omnidirectional charging proportion increases at a relatively slower trend when the charger density becomes larger. In addition, the average marginal gain of omnidirectional charging proportion decreases when  $A_o$  or  $A_s$  increases, which is similar to the case of omnidirectional charging probability when increasing  $A_o$  in Sec. VI-C1.

3) Detection time: The simulation results show that our algorithm outperforms other algorithms by at least  $1.2 \times$  as the charger density varies from 1 to 8. To make the difference between the algorithms more prominent, we have all detection time results being divided by the time required for the MCS extraction algorithm when charger density equals 1. As shown in Fig. 14, our MCS extraction algorithm always achieves the best performance. On average, our algorithm outperforms the omnidirectional coverage algorithm, exhaustive algorithms with granularity 0.02 m and 0.01 m by  $1.2 \times$ ,  $41.4 \times$ , and 145.2×, respectively. The reason why our algorithm is superior to the omnidirectional coverage algorithm is that it only extracts those covering charger sets that are potentially MCSs, while on the contrary the omnidirectional coverage algorithm needs to enumerate all possible covering charger sets.

#### D. Insights

In this subsection, we show the impact of the uniformness of distribution for position or orientation of chargers on omnidirectional charging. We take the omnidirectional charging proportion as the metric for evaluation. Suppose there are 100 chargers distributed in a  $10 m \times 10 m$  region with  $A_o = \frac{2\pi}{3}$  and  $A_s = \pi$ . Their position follows 2D Gaussian distribution with both x- and y- coordinates being randomly selected from a Gaussian distribution with  $\mu_1 = 5$ , and their orientations follow a Gaussian distribution with  $\mu_2 = 0$ . We vary the standard deviation  $\sigma_1$  for x- and y- coordinates from 0.1 to 3 and the standard deviation  $\sigma_2$  for the orientation from 0.1 to 2, and depict the results in Fig. 15. Notice that each point on the surface denotes an average value of 100 experimental results. We observe that the omnidirectional charging proportion increases monotonically with either  $\sigma_1$ or  $\sigma_2$ . Indeed, when  $\sigma_1$  or  $\sigma_2$  increases, the distribution of position or orientation appears more random, and approaches to uniform distribution. Thus we claim that the uniformness of distribution for position or orientation of chargers benefits omnidirectional charging.

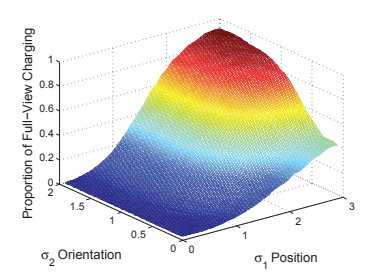
#### VII. FIELD EXPERIMENTS

In this section, we conduct field experiments to evaluate our theoretical findings.

#### A. Testbed

As shown in Fig. 16, our testbed consists of eight TX91501 power transmitters produced by Powercast [20], and one rechargeable sensor node. The chargers are placed on the vertices and middle points of edges of a  $2.4 \, m \times 2.4 \, m$  square area, and their orientations for charger 1 to 8 with respect to the right horizontal direction are 345°, 270°, 195°, 0°, 180°, 75°, 90° and 105°, respectively. The wireless rechargeable sensor node is sequentially placed at  $6 \times 6$  grid points in a  $0.6 m \times 0.6 m$  square area located right in the center of the field, and therefore the distance between neighboring grid points is 0.12 m. For each point, we collect at least 20 data records of the charging power of the node and compute its mean value every 20° for its orientation. Therefore, we obtain in total  $36 \times 18$  data records. Moreover, there are also a laptop and a connected AP that collects the charging power information from the sensor node and reports it to the laptop. B. Experimental Results

#### Fig. 17 shows an instance of our experimental and simulation results with $P_{th} = 7 \, mW$ . The grey dots represent points of all related strategies for all extracted MCSs. The blue



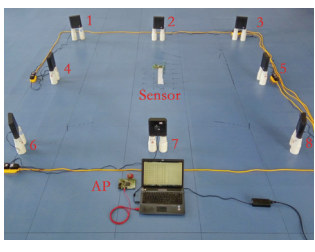


Fig. 15: Illustration of insights

Fig. 16: Testbed

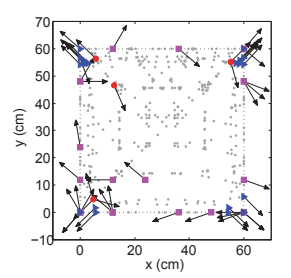
triangles and red circles with their attached arrows denote the related strategies with charging power less than  $P_{th}$ , called unqualified strategies, for MCSs obtained by performing the MCS extraction algorithm for point cases as done for Case III in the proof to Theorem 4.5 and MCSs that can be directly determined as done for Case I and Case II, respectively. And the pink squares with arrows stand for that for field experiments. On one hand, the simulation results do reflect the distribution of unqualified strategies of the real situation both in terms of positions and orientations, and those strategies are mainly clustered at the four corners of the field area. The discrepancy between field and simulation results is mainly due to the non-negligible mismatch between the charging models and the reality. On the other hand, there are four strategies marked in red circles can be easily computed in our case, which, however, need to be treated as for Case III in the omnidirectional coverage algorithm. This partly explains why our algorithm outperforms the omnidirectional coverage algorithm. Next, we quantitatively evaluate the accuracy of our simulation results by using the correct ratio of the "nearest" neighbors of the obtained unqualified strategies by our algorithm that are consistent with the experimental results. The "nearest" neighbor of a strategy is defined as the data record among  $36 \times 18$  ones that has the closest position and closest orientation with the given strategy. Fig. 18 shows that when  $P_{th}$  varies from  $11 \, mW$  to  $15 \, mW$ , the correct ratio is invariably larger than 93.6%, which validates the performance of our algorithm.

#### VIII. CONCLUSION

In this paper, we make the following four key contributions. First, to the best of our knowledge, we are the first to propose and study the omnidirectional charging problem, and we first establish the empirical directional charging model involving chargers and devices. Second, we propose an efficient method to detect whether a target area achieves omnidirectional charging under a given charger deployment. Third, we derive an upper bound of the omnidirectional charging probability for a random deployment. Fourth, we conducted simulations and field experiments to verify our theoretical findings. The results show that our algorithm outperforms comparison algorithms including an adapted algorithm based on the full-view coverage detection algorithm in wireless sensor networks by at least 1.2×, and the consistency degree of our theoretical results and field experimental results is larger than 93.6%.

#### ACKNOWLEDGMENT

This work is partially supported by the National Science Foundation under Grant Numbers CNS-1318563, CNS-



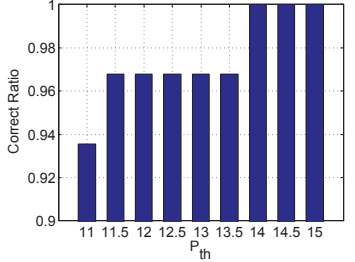


Fig. 17: Field vs. simulation

Fig. 18: Correct ratio vs.  $P_{th}$ 

1524698, and CNS-1421407, and the National Natural Science Foundation of China under Grant Numbers 61502229, 61472184, 61321491, 61672353, 61472252, 61321491, and 61133006, and the Jiangsu High-level Innovation and Entrepreneurship (Shuangchuang) Program, and China 973 projects (2014CB340303).

#### REFERENCES

- [1] A. P. Sample et al., "Design of an rfid-based battery-free programmable sensing platform," IEEE Transactions on Instrumentation and Measurement, vol. 57, no. 11, pp. 2608-2615, 2008.
- [2] R. Zhang et al., "MIMO broadcasting for simultaneous wireless information and power transfer," IEEE Transactions on Wireless Communications, vol. 12, no. 5, pp. 1989-2001, 2013.
- [3] Z. Ding et al., "Application of smart antenna technologies in simultaneous wireless information and power transfer," IEEE Communications Magazine, vol. 53, no. 4, pp. 86-93, 2015.
- "http://www.powercastco.com/pdf/p2110-evb-reva.pdf."
- [5] T. Bai et al., "Coverage and rate analysis for millimeter-wave cellular networks," IEEE Transactions on Wireless Communications, vol. 14, no. 2, pp. 1100-1114, 2015.
- [6] L. Wang et al., "Millimeter wave power transfer and information transmission," Globecom, 2015.
- [7] K. Huang et al., "Enabling wireless power transfer in cellular networks: architecture, modeling and deployment," IEEE Transactions on Wireless Communications, vol. 13, no. 2, pp. 902-912, 2014.
- Z. Qin et al., "Throughput analysis for compressive spectrum sensing
- with wireless power transfer," *Globecom*, 2015.
  [9] S. He *et al.*, "Energy provisioning in wireless rechargeable sensor networks," IEEE Transactions on Mobile Computing, vol. 12, no. 10, pp. 1931-1942, 2013.
- S. Zhang et al., " $p^3$ : Joint optimization of charger placement and power allocation for wireless power transfer," in INFOCOM. IEEE, 2015, pp. 2344-2352
- [11] H. Dai et al., "Scape: Safe charging with adjustable power," in ICDCS. IEEE, 2014, pp. 439-448.
- -, "Safe charging for wireless power transfer," in INFOCOM. IEEE, 2014, pp. 1105-1113.
- [13] S. Nikoletseas et al., "Low radiation efficient wireless energy transfer in wireless distributed systems," in ICDCS. IEEE, 2015, pp. 196-204.
- Z. Chang et al., "Localization in wireless rechargeable sensor networks using mobile directional charger," in GLOBECOM. IEEE, 2015, pp.
- [15] Y. Wang et al., "On full-view coverage in camera sensor networks," in INFOCOM. IEEE, 2011, pp. 1781-1789.
- [16] Y. Wu et al., "Achieving full view coverage with randomly-deployed heterogeneous camera sensors," in ICDCS. IEEE, 2012, pp. 556-565.
- [17] Y. Hu et al., "Critical sensing range for mobile heterogeneous camera sensor networks," in INFOCOM. IEEE, 2014, pp. 970-978.
- [18] Y. Wang et al., "Barrier coverage in camera sensor networks," in MobiHoc, no. 12. ACM, 2011.
- [19] Z. Yu et al., "Local face-view barrier coverage in camera sensor networks," in INFOCOM. IEEE, 2015, pp. 684-692.
- [20] "www.powercastco.com."
- [21] H. Dai et al., "Radiation constrained wireless charger placement," in INFOCOM. IEEE, 2016, pp. 1-9.
- W. Feller, An introduction to probability theory and its applications. John Wiley & Sons, 2008, vol. 2.